Dalton Transactions

PAPER

View Article Online
View Journal | View Issue

Cite this: *Dalton Trans.*, 2015, **44**, 9839

A mechanistic study of $Pd(OAc)_2$-catalyzed intramolecular C–H functionalization reaction involving CO/isonitrile insertion†

Honghong Gu,[a] Zhiping Qiu,[a] Zhongchao Zhang,[a] Juan Li*[a] and Bo Yan*[b]

The mechanism of the $Pd(OAc)_2$-catalyzed intramolecular C–H functionalization reaction involving CO/isonitrile insertion was investigated with the aid of density functional theory calculations at the B3LYP level. The similarity between the CO and isonitrile systems includes the following: (1) the anagostic bonding mechanism rather than the concerted metallation–deprotonation (CMD) mechanism is operative for the C–H cleavage step, (2) the CO/isonitrile insertion step is rate-determining, and (3) the C–H activation and CO/isonitrile insertion steps are accomplished with Pd(II) and Pd(III), respectively. For the reaction including isonitrile insertion, the arene C–H activation step occurs after deprotonation of the imino group. However, for reaction including CO insertion, the arene C–H activation step is the first step of the reaction mechanism. The difference between CO and isonitrile systems in the reaction mechanism can be attributed to the difference in the oxidants used. In the reaction including isonitrile insertion, the high endergonicity of the oxidation step suppresses prior C–H activation and favors prior deprotonation of the imino group. In the reactions including CO insertion, the low endergonicity of the oxidation step allows prior C–H activation to occur.

Received 13th February 2015,
Accepted 20th April 2015

DOI: 10.1039/c5dt00666j

www.rsc.org/dalton

1. Introduction

The transition metal represents a well-established tool for the C–H heterofunctionalization due to its central role in the functionalization of organic substrates.[1] Among the reported methods, the directing group (DG) approach is particularly important since it can selectively activate specific C–H bonds.[2] CO and isonitrile can be used as an effective carbonyl[3] and imidoylative[4] source in palladium-catalyzed cascade reactions to increase the molecular complexity of the products. Because isocyanides are isoelectronic to CO, they show similar reactivity for insertion into Pd–C bonds and undergo similar fundamental transformations. The palladium-catalyzed intramolecular C–H functionalization reaction involving isonitrile[5] or CO[6] insertion has been reported by Zhu *et al.*, as shown in Scheme 1. The general mechanism is proposed as catalytic cycles of C–H activation, CO/isocyanide insertion, and reductive elimination. The kinetic isotope experiments[4] for isonitrile insertion showed that aromatic C–H bond activation is not involved in the rate-determining step.

Several important questions remain to be answered about the palladium-catalyzed C–H functionalization reaction including CO/isocyanide insertion. First, the role of a palladium center in the C–H activation step needs to be demonstrated because there are several mechanisms proposed for the C–H activation step including electrophilic aromatic substitution through a Wheland palladium arenium intermediate,[7] concerted metallation–deprotonation (CMD)[8] or σ-bond metathesis[9] in which formation of the palladium–carbon bond and the proton abstraction from the C–H bond occur simultaneously, formation of $C–H\cdots Pd^{II}$ agostic or anagostic species,[10] and oxidative addition of Ar–H to the palladium.[11] More importantly, an important issue that needs to be addressed is whether a Pd(III) intermediate is involved in the C–H-bond-breaking step or isonitrile/CO insertion step. In addition, the sequence of steps is not known.

In this paper, with the aid of density functional theory (DFT) calculations, we investigate in detail the palladium-catalyzed intramolecular C–H functionalization reaction involving isonitrile and CO insertion to solve the questions mentioned above. We hope that the insight provided here will be helpful for understanding the role of the palladium center and reactivity difference between isonitrile and CO.

[a]*Department of Chemistry, Jinan University, Huangpu Road West 601, Guangzhou, Guangdong 510632, P. R. China. E-mail: tchjli@jnu.edu.cn, yanbo2007@gig.ac.cn*
[b]*State Key Laboratory of Organic Geochemistry, Guangzhou Institute of Geochemistry, Chinese Academy of Sciences, Guangzhou 510640, China*

† Electronic supplementary information (ESI) available: Calculated imaginary frequencies of all transition state species and tables giving Cartesian coordinates and electronic energies of all calculated structures. See DOI: 10.1039/c5dt00666j

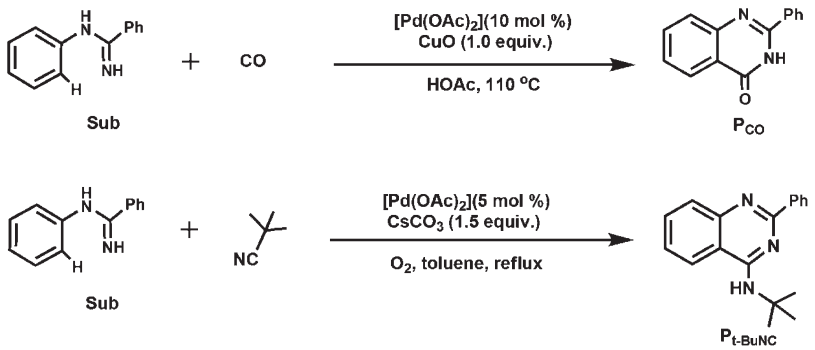

Scheme 1 Palladium-catalyzed intramolecular C–H functionalization reactions involving isonitrile and CO.

2. Computational details

All of the species in this study were optimized using DFT at the B3LYP level.[12] Frequency calculations were also performed at the same level of theory to identify all of the stationary points as minima (zero imaginary frequencies) or transition states (one imaginary frequency), and to provide the free energies at 298.15 K. Transition states were located using the Berny algorithm. Intrinsic reaction coordinates (IRCs)[13] were calculated for the transition states to confirm that the saddle point connected the correct reactant and product on the potential energy surface. The Pd atom was described using the LANL2DZ basis set, including a double-valence basis set with the Hay and Wadt effective core potential.[14] Polarization functions were added for Pd (ζ_f = 1.472).[15] The 6-31G*[16] basis set was used for the other atoms. To test the solvent effect, we performed single-point energy calculations using the polarizable continuum model (PCM)[17] for all gas phase optimized species. In the PCM calculations, larger basis sets were used: the LanL2TZ(f) basis set[18] for the Pd atom and the 6-311++G** basis set for the other atoms. The nonelectrostatic terms (cavity–dispersion–solvent–structure terms) of the solvation energy were calculated using the SMD model[19] to give the final fully corrected free energies (ΔG_{sol}) in AcOH and toluene for the CO and isonitrile systems, respectively. All of the calculations were performed using the Gaussian 09 package.[20] All of the energies presented in the text are relative free energies with respect to the isolated catalyst and substrate. The turnover frequency (TOF) determining intermediate (TDI) and TOF determining transition state (TDTS) according to the energetic span model developed by Shaik *et al.*[21] are considered.

3. Results and discussion

3.1. Mechanisms for CO insertion

3.1.1. Consecutive C–H activation, CO insertion, reductive elimination, and deprotonation of amino group steps. First, we calculated the pathway according to the mechanism proposed by Zhu *et al.*, as shown in Fig. 1. The initial coordination of the *N*-arylamidine to Pd was exergonic by 9.6 kcal mol^{-1}. The possible mechanisms for the C–H activation of arene were theoretically investigated: CMD, oxidative addition, σ-bond metathesis, and anagostic bonding. In the CMD, oxidative addition, and σ-bond metathesis mechanisms, the transition states for benzene C–H activation are about 35.2, 30.8 and 37.0 kcal mol^{-1} above of the energy of **I**. We found intermediate **II**, in which Pd···C = 2.426 Å, C–H = 1.096 Å, H···Pd = 2.272 Å, and Pd···H–C = 84.5°. This indicates that the weak C–H···Pd bonding interaction should be anagostic, according to Braga *et al.*[22] Moreover, natural bond orbital charge analysis showed that the change in charge from **I** to **TSI** mainly occurred at the activating C–H bond. During the **I** → **TSI** process, the negative charge of the C atom increased from −0.253 to −0.419, while the positive charge of the H atom increased from 0.258 to 0.384. In addition, the maximum increase in positive charge on any of the ring carbon atoms was only +0.069, indicating that a Wheland intermediate is not involved in the C–H-bond-breaking step. The anagostic bonding mechanism was found to have the lowest reaction barrier (15.0 kcal mol^{-1}). Then, coordination of a CO molecule to **III** can form intermediate $\mathbf{IV_{CO}}$. The isomer of $\mathbf{IV_{CO}}$ with CO *trans* to the phenyl group was calculated to be less stable than $\mathbf{IV_{CO}}$ by 3.7 kcal mol^{-1}. In the discussion below, we only consider the pathway starting from the more stable $\mathbf{IV_{CO}}$ isomer. The following step is oxidation. $\mathbf{IV_{CO}}$ can be oxidized by CuO to afford the Pd(III) intermediate $\mathbf{V_{CO}}$ according to eqn (1) (ΔG = 3.8 kcal mol^{-1}).

$$\mathrm{IV_{CO}} + \mathrm{CuO} + \mathrm{AcOH} \rightarrow \mathrm{V_{CO}} + \frac{1}{2}\mathrm{Cu_2O} + \frac{1}{2}\mathrm{H_2O} \qquad (1)$$

Subsequently, CO insertion into the Pd–C bond of $\mathbf{V_{CO}}$ is realized *via* $\mathbf{TSII_{CO}}$ with an energy barrier of 17.7 kcal mol^{-1} to generate the seven-membered palladium cycle $\mathbf{VI_{CO}}$. From $\mathbf{VI_{CO}}$, reductive elimination *via* the three-membered-ring transition state $\mathbf{TSIII_{CO}}$ gives the C–N-coupling product $\mathbf{VII_{CO}}$. The free energy of $\mathbf{TSIII_{CO}}$ is only 2.6 kcal mol^{-1} higher than that of $\mathbf{VI_{CO}}$. There is a hydrogen-bonding interaction between the NH group of $\mathbf{VII_{CO}}$ and the acetate ligand. Finally, the Pd(II) center is reduced to a Pd(I) species through deprotonation of the amino group with almost no energy barrier. The calculated results indicate that the activation barrier for CO insertion

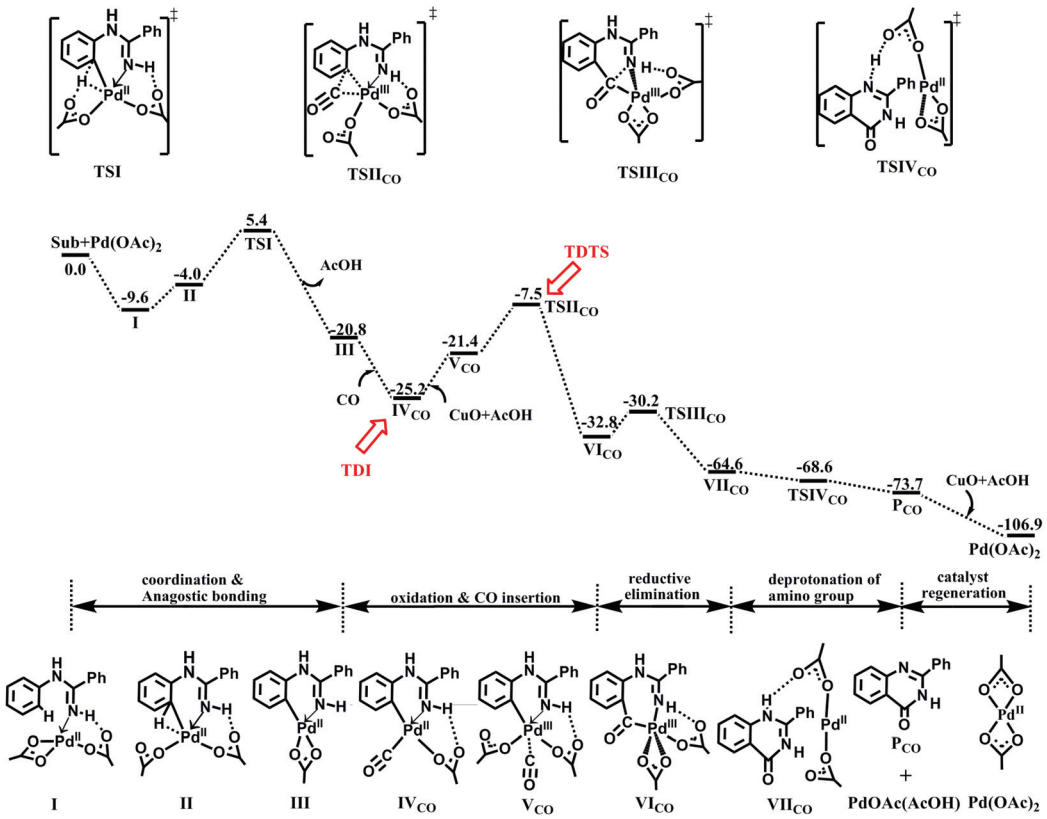

Fig. 1 Calculated energy profiles for the pathway (consecutive C–H activation, CO insertion, reductive elimination, and deprotonation of the amino group). Solvent-corrected free energies are given in kcal mol^{-1}. The TDI and TDTS according to the energetic span model are shown.

(17.7 kcal mol^{-1}) is slightly higher than that for C–H bond activation (15.0 kcal mol^{-1}).

3.1.2. C–H-bond-breaking step after deprotonation of the amino group. Intermediate **VIII**, which is the starting point for the C–H-bond-breaking step, as shown in Fig. 2, can be generated from the deprotonation of the amino group. The CMD transition state was not located for the C–H-bond-breaking step. The transition states of the oxidative addition and σ-bond metathesis mechanisms (49.1 and 55.9 kcal mol^{-1}) are significantly higher in energy than that of the anagostic bonding mechanism (32.8 kcal mol^{-1}). For anagostic intermediate **IX**, Pd···C = 2.368 Å, C–H = 1.090 Å, H···Pd = 2.412 Å, and Pd···H–C = 74.6°. However, the transition state **TSV** of the anagostic bonding mechanism has a much higher energy barrier relative to **I** (42.4 kcal mol^{-1}), which indicates that the pathways where the deprotonation of the amino group precedes the C–H-bond-breaking step are impossible.

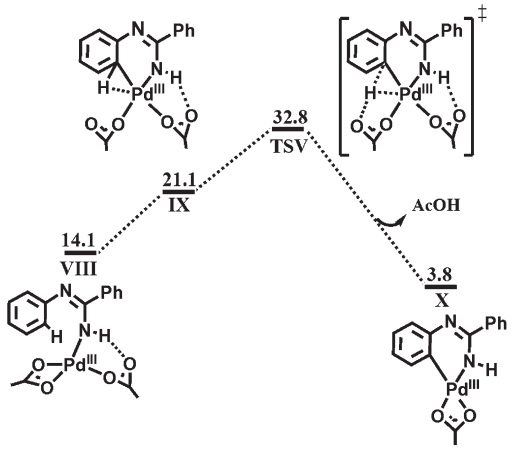

Fig. 2 Calculated energy profiles for the C–H activation step (**VIII**→**X**) after deprotonation of the amino group for the CO system. Solvent-corrected free energies are given in kcal mol^{-1} (AcOH is the solvent).

3.1.3. C–H-bond-breaking step after deprotonation of the imino group. Fig. 3 shows the calculated potential energy profile for the C–H-bond-breaking step after deprotonation of the imino group. **I** releases an AcOH molecule and forms **XI**, which is then oxidized to afford intermediate **XIII**. For the arene C–H activation step, the anagostic bonding mechanism is found to have an energy barrier of 22.6 kcal mol^{-1} relative to **I**, making this pathway unlikely. The alternative intramolecular C–H activation pathways of CMD, oxidative addition, and σ-bond metathesis were also considered, but were far less accessible with calculated energy barriers of 25.7, 42.4, and 40.7 kcal mol^{-1}, respectively. Therefore, the calculated results

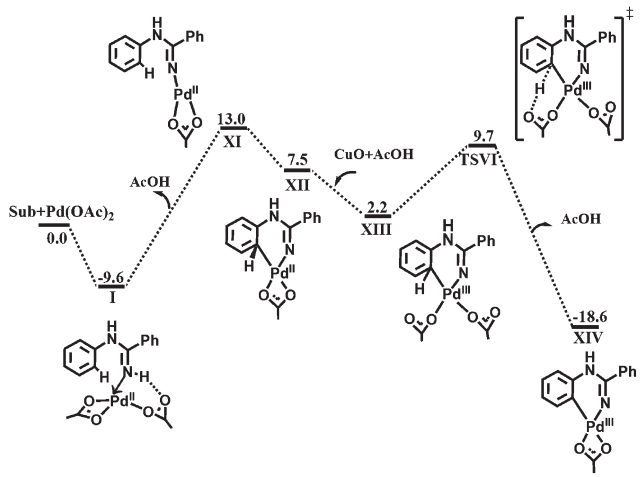

Fig. 3 Calculated energy profiles for the pathway where the C–H-bond-breaking step is after deprotonation of the imino group for the CO system. Solvent-corrected free energies are given in kcal mol^{-1} (AcOH solvent).

indicate that the C–H-bond-breaking step after deprotonation of the amino/imino group is unfavorable, because the Pd(III) center generated from the deprotonation of the amino/imino group step is electron deficient and disfavors the subsequent C–H activation process. C–H activation before deprotonation of the amino/imino group can prevent this problem.

3.1.4. Pathways where C–H activation is the first step. As discussed above, the C–H-bond-breaking step is more favorable as the first step than deprotonation of the imino/amino group. After C–H activation, CO can directly insert into the Pd–C bond *via* transition states $\mathbf{TSII_{CO}}$ (Pd(III) species) and $\mathbf{TSII'_{CO}}$ (Pd(II) species), as shown in Scheme 2. CO insertion can also be realized *via* transition states $\mathbf{TSVII_{CO}}$ (Pd(IV) species) and $\mathbf{TSVIII_{CO}}$ (Pd(III) species) when C–H and N–H activation processes are completed. However, the transition states $\mathbf{TSII'_{CO}}$, $\mathbf{TSVII_{CO}}$, and $\mathbf{TSVIII_{CO}}$ with energy barriers of 32.0, 40.2, and 56.8 kcal mol^{-1} relative to $\mathbf{IV_{CO}}$, respectively, are less favorable than $\mathbf{TSII_{CO}}$ with an energy barrier of 17.7 kcal mol^{-1}. From Scheme 2, we can conclude that CO insertion is most favorable after C–H cleavage with Pd(III). The reason is as follows. The five-coordinated transition states $\mathbf{TSII_{CO}}$ and $\mathbf{TSVII_{CO}}$ favor the out-of-plane CO insertion step. In contrast, the four-coordinated transition states $\mathbf{TSII'_{CO}}$ and $\mathbf{TSVIII_{CO}}$ have to force CO into the axial position, thereby increasing the energy barrier for the CO insertion step. In addition, an increase in the palladium oxidation state can enhance the covalency of the Pd–C interaction, and thus disfavors the CO insertion step.

3.2. Mechanisms for isonitrile insertion

3.2.1. Consecutive deprotonation of the imino group, C–H activation, isonitrile insertion, reductive elimination, H migration, and deprotonation of the amino group steps. As shown in Fig. 4, coordination of the amidine to the Pd atom to give **I** is exergonic by 7.4 kcal mol^{-1}. The relative energy of **I** in Fig. 4 is different from that in Fig. 1 because AcOH and toluene solvents are used in CO and isonitrile systems, respectively. Deprotonation of the imino group first occurs, releasing an AcOH molecule and forming intermediate **XI**. After deprotonation of the imino group, we investigated the two oxidation states Pd(II) and Pd(III) for C–H cleavage. For Pd(II), an isonitrile molecule coordinates to the Pd center and the acetate ligand changes from bidentate to monodentate. For the following C–H cleavage step, we could not locate the CMD transition state for the C–H cleavage step but obtained the stepwise transition state $\mathbf{TSI_{t\text{-}BuNC}}$. The IRC calculations showed that the transition

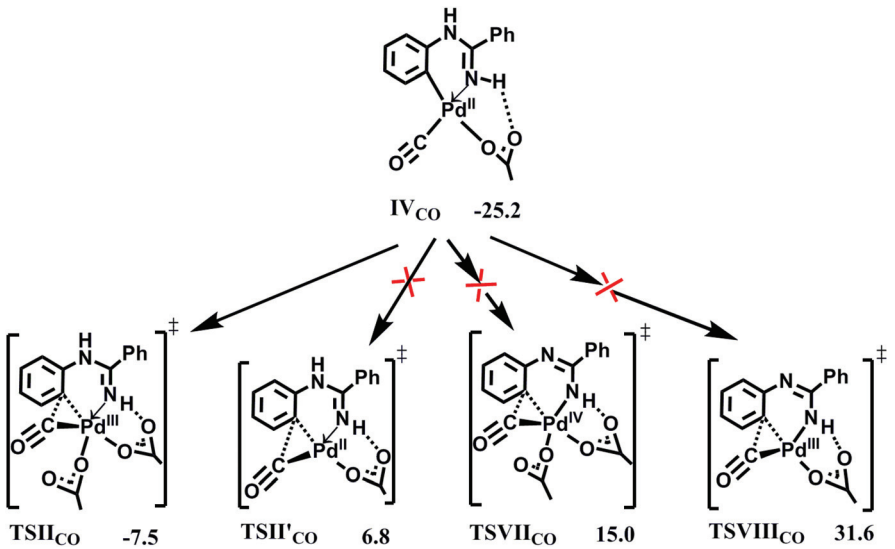

Scheme 2 Transition states for CO insertion with free energies relative to the isolated catalyst and substrate.

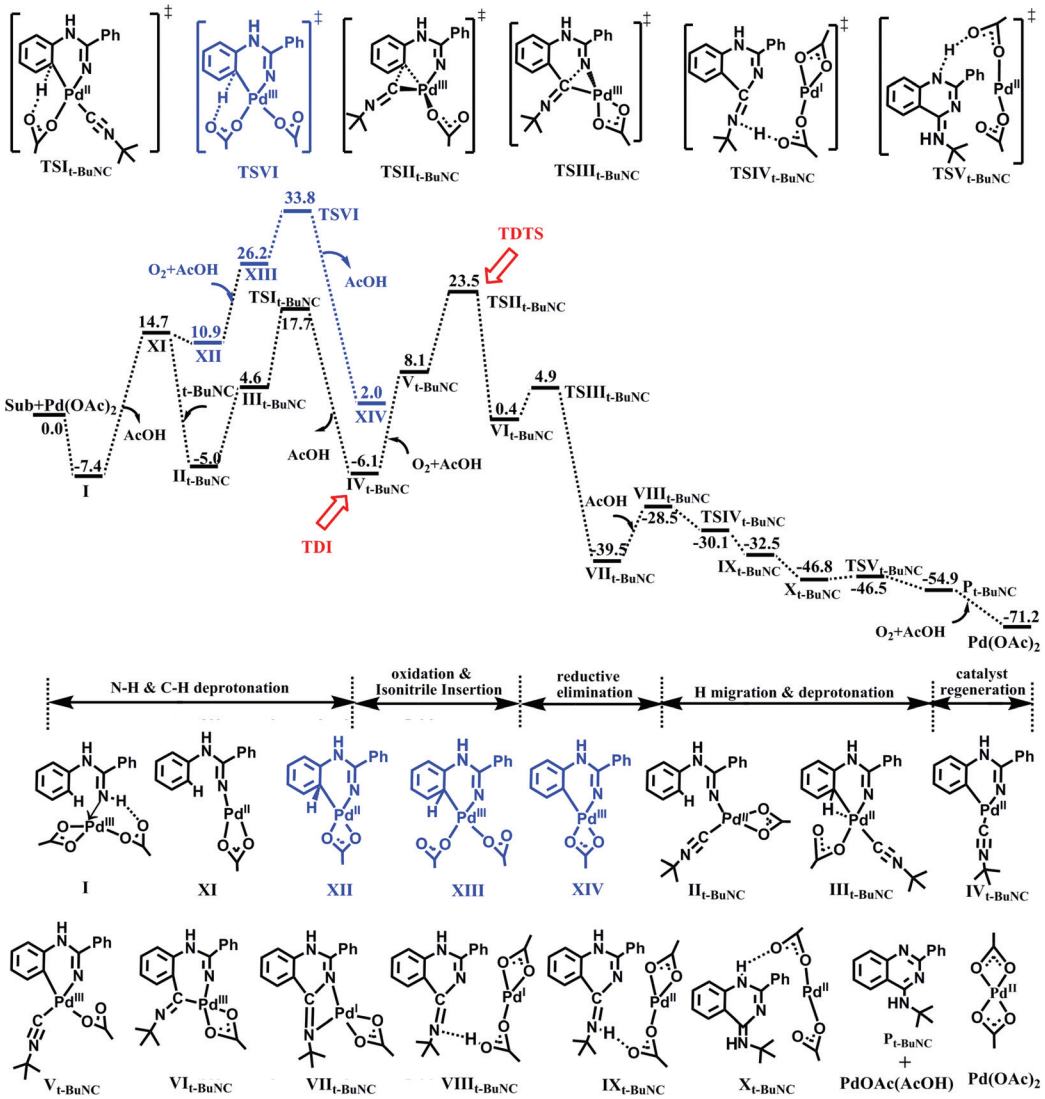

Fig. 4 Calculated energy profile for deprotonation of the imino group, C–H activation, isonitrile insertion, reductive elimination, H migration, and deprotonation of the amino group pathway. Solvent-corrected free energies are given in kcal mol^{-1} (toluene solvent). The TDI and TDTS according to the energetic span model are shown.

structure **TSI**$_{t\text{-BuNC}}$ connects the anagostic bonding intermediate **III**$_{t\text{-BuNC}}$ and the AcOH-eliminated product **IV**$_{t\text{-BuNC}}$. For the anagostic intermediate **III**$_{t\text{-BuNC}}$, Pd···C = 2.335 Å, C–H = 1.091 Å, H···Pd = 2.399 Å, and Pd···H–C = 73.5°. For Pd(III), the CMD, oxidative addition, and σ-bond metathesis pathways were ruled out because they significantly increased the energies of transition states relative to **I** by 48.9, 60.9, and 62.2 kcal mol^{-1}, respectively. The **III**$_{t\text{-BuNC}}$ → **IV**$_{t\text{-BuNC}}$ step is exergonic by 10.7 kcal mol^{-1}, and the energy barrier is 13.1 kcal mol^{-1}. **IV**$_{t\text{-BuNC}}$ is then oxidized to **V**$_{t\text{-BuNC}}$ by O_2 according to eqn (2) with an energy barrier of 14.2 kcal mol^{-1}.

$$\mathrm{IV}_{t\text{-BuNC}} + \frac{1}{4}\mathrm{O_2} + \mathrm{AcOH} \rightarrow \mathrm{V}_{t\text{-BuNC}} + \frac{1}{2}\mathrm{H_2O} \qquad (2)$$

Then, the insertion of the coordinated isonitrile into the C–Pd bond in **V**$_{t\text{-BuNC}}$ gives complex **VI**$_{t\text{-BuNC}}$ *via* the transition state **TSII**$_{t\text{-BuNC}}$ with an energy barrier of 15.4 kcal mol^{-1}. **VI**$_{t\text{-BuNC}}$ gives rise to the C–N coupling product **VII**$_{t\text{-BuNC}}$ by reductive elimination. The free energy of **TSIII**$_{t\text{-BuNC}}$ is 4.5 kcal mol^{-1} higher than that of **VI**$_{t\text{-BuNC}}$. In the following step, an AcOH molecule coordinates to Pd to form **VIII**$_{t\text{-BuNC}}$, in which there is a hydrogen-bonding interaction between the isonitrile group and the AcOH ligand. From **VIII**$_{t\text{-BuNC}}$, H migration from the AcOH ligand to the isonitrile group can be realized *via* **TSIV**$_{t\text{-BuNC}}$ to give Pd(II) intermediate **IX**$_{t\text{-BuNC}}$. Formal 1,5-H migration from the amine group to the isonitrile group in **VII**$_{t\text{-BuNC}}$, as proposed by experiment,[5] is not possible because the activation barrier is as high as 78.2 kcal mol^{-1}. Finally, deprotonation of the amino group will lead to the 4-aminoquinazoline product with almost no energy barrier. The isonitrile insertion step is rate-determining and the overall energy barrier for the pathway is 30.9 kcal mol^{-1}.

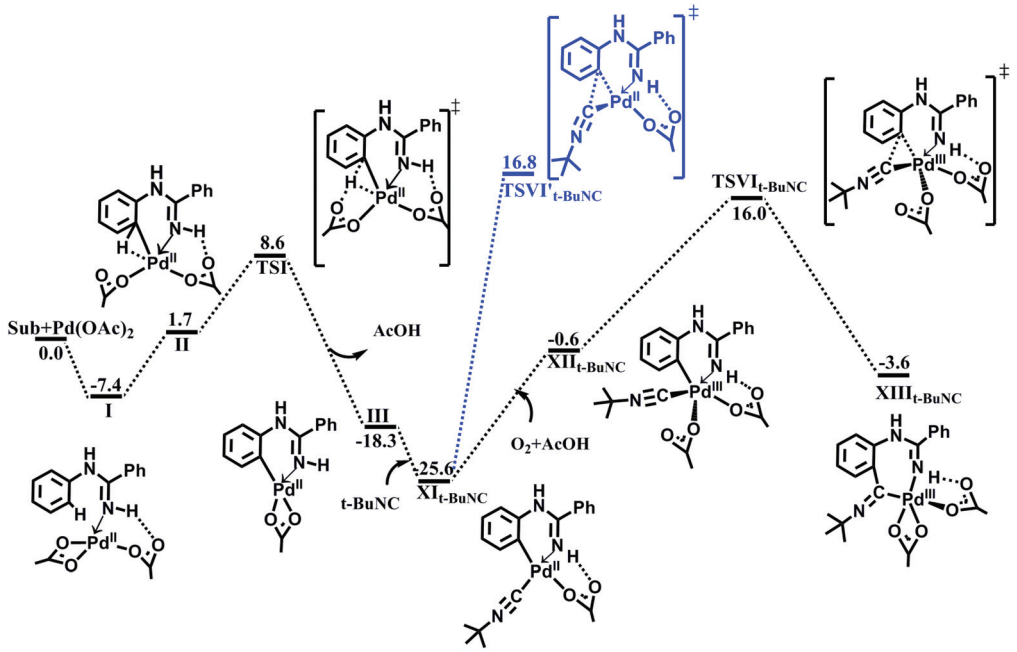

Fig. 5 Calculated energy profile for the consecutive C–H-bond-breaking and isonitrile insertion step. Solvent-corrected free energies are given in kcal mol^{-1} (toluene solvent).

3.2.2. Other pathways. The Pd(II)-catalyzed intramolecular C–H functionalization reaction involving isonitrile insertion can also occur in a similar way to the most favorable pathway for CO insertion shown in Fig. 1. As discussed above, the anagostic bonding mechanism is most favorable for the C–H-bond-breaking step. After the C–H-bond-breaking step, we investigated the two oxidation states Pd(II) and Pd(III) for the isonitrile insertion reaction shown in Fig. 5. However, the transition states **TSVI**$_{t\text{-BuNC}}$ and **TSVI'**$_{t\text{-BuNC}}$ are about 41.6 and 42.4 kcal mol^{-1} higher in energy than **XI**$_{t\text{-BuNC}}$, respectively, which shows that isonitrile insertion after C–H cleavage is less accessible.

We also investigated the pathway in which C–H cleavage and deprotonation of the amino group precede isonitrile insertion. However, the two transition states **TSVII**$_{t\text{-BuNC}}$ and **TSVII'**$_{t\text{-BuNC}}$ for isonitrile insertion (Scheme 3) have high energy barriers of 41.6 and 37.3 kcal mol^{-1} relative to **I**, respectively, and can be ruled out. All of these results suggest that the pathway shown in Fig. 4 is the most favorable with an overall barrier of 30.9 kcal mol^{-1}, which is accessible at the experimental temperature (about 383 K). Aromatic C–H bond activation is not involved in the rate-determining step, which is consistent with experimental observations.[5]

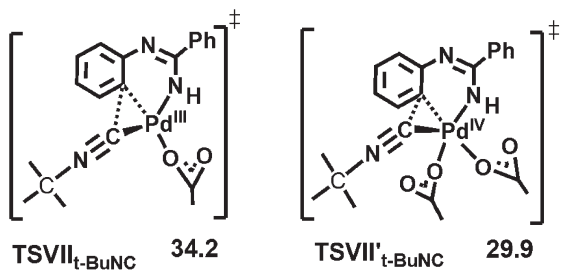

Scheme 3 Structures of TSVII$_{t\text{-BuNC}}$ and TSVII'$_{t\text{-BuNC}}$ with free energies in kcal mol^{-1}.

3.3. Comments on the differences in the reaction mechanisms of CO and isonitrile

We propose the catalytic cycles in Scheme 4 for the palladium-catalyzed intramolecular C–H functionalization reaction involving isonitrile and CO insertion. As shown in Scheme 4, the arene C–H activation step is the first step for the CO system but after deprotonation of the imino group for the isonitrile system. The reason for the difference between the CO and isonitrile systems is as follows. Compared with the CO system, the oxidation step of the isonitrile system is much more endergonic, which will greatly increase the energy barrier for the isonitrile insertion process. Moreover, the Pd center changes from three-coordinated to four-coordinated for **IV**$_{t\text{-BuNC}}$ → **V**$_{t\text{-BuNC}}$, while the Pd center changes from the four-coordinated to five-coordinated for **XI**$_{t\text{-BuNC}}$ → **XII**$_{t\text{-BuNC}}$. Obviously, the change from **IV**$_{t\text{-BuNC}}$ to **V**$_{t\text{-BuNC}}$ is easy to achieve because Pd is most stable as a four-coordinated complex. Therefore, the higher endergonicity of the oxidation step in Fig. 5 excludes it as a possible reaction pathway (ΔG = 14.2 kcal mol^{-1} for **IV**$_{t\text{-BuNC}}$ → **V**$_{t\text{-BuNC}}$ in Fig. 4, ΔG = 25.0 kcal mol^{-1} for **XI**$_{t\text{-BuNC}}$ → **XII**$_{t\text{-BuNC}}$ in Fig. 5).

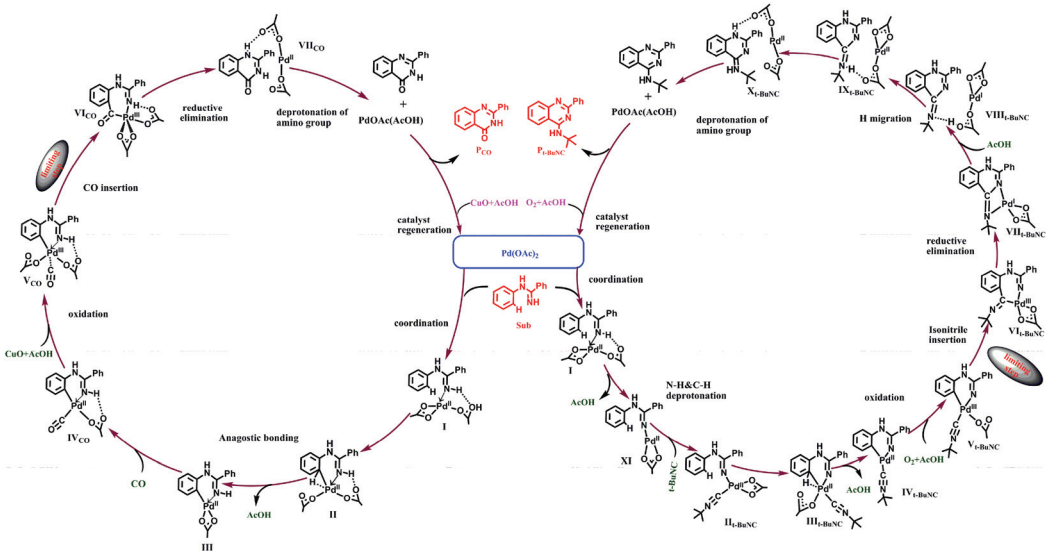

Scheme 4 Proposed catalytic cycle of palladium-catalyzed intramolecular C–H functionalization *reaction* involving isonitrile or CO insertion.

4. Conclusion

The reaction mechanisms of $Pd(OAc)_2$-catalyzed intramolecular C–H functionalization reaction involving CO/isonitrile insertion have been studied using the density functional B3LYP method. The similarities between the CO and isonitrile systems include the following. (1) The anagostic bonding mechanism is more feasible than CMD, σ-bond metathesis, and oxidation addition for the C–H cleavage step. (2) The rate-determining transition state corresponds to CO or isonitrile insertion (overall activation free energy barrier of 17.7 or 30.9 kcal mol^{-1}, respectively). (3) The C–H activation step is accomplished with Pd(II) and the CO/isonitrile insertion step is accomplished with Pd(III).

The mechanism of intramolecular $C(sp^2)$–H carboxamidation is in the following sequence: C–H cleavage, CO insertion, reductive elimination, and deprotonation of the amino group. However, the mechanism of C–H functionalization with isonitrile insertion proceeds according to deprotonation of the imino group, C–H activation, isonitrile insertion, reductive elimination, H migration, and deprotonation of the amino group. The low endergonicity of the oxidation step in the reactions including CO insertion allows a prior C–H activation step to occur. The high endergonicity of the oxidation step in the reaction including isonitrile insertion, which significantly influences the overall energy demand of the rate-determining step (*i.e.*, isonitrile insertion), prevents a prior C–H activation step.

Acknowledgements

This work was supported by the National Natural Science Foundation of China (grant no. 21103072), Guangdong Natural Science Funds for Distinguished Young Scholar (no. S2013050014122), the Fundamental Research Funds for the Central Universities (Grant No. 21615405) and the high-performance computing platform of Jinan University.

References

1 For recent reviews on the synthesis of heterocycles *via* transition-metal catalyzed C–H functionalization, see: (*a*) P. Tansandote and M. Lautens, *Chem. – Eur. J.*, 2009, **15**, 5874–5883; (*b*) B. J. Stokes and T. G. Driver, *Eur. J. Org. Chem.*, 2011, 4071–4088; (*c*) E. M. Beccalli, G. Broggini, A. Fasana and M. Rigamonti, *J. Organomet. Chem.*, 2011, **696**, 277–295; (*d*) M. Zhang, *Adv. Synth. Catal.*, 2009, **351**, 2243–2270; (*e*) F. Liron, J. Oble, M. M. Lorion and G. Poli, *Eur. J. Org. Chem.*, 2014, 5863–5883; (*f*) G. Liu and Y. Wu, *Top. Curr. Chem.*, 2010, **292**, 195–209.

2 N. Chatani, *Directed Metallation*, in *Topics in Organometallic Chemistry*, Springer Verlag, Berlin, Germany, 2007, vol. 24.

3 (*a*) T. Vlaar, E. Ruijter and R. V. A. Orru, *Adv. Synth. Catal.*, 2011, **353**, 809–841; (*b*) X. F. Wu, H. Neumann and M. Beller, *Chem. Rev.*, 2013, **113**, 1–35.

4 T. Vlaar, E. Ruijter, B. U. W. Maes and R. V. A. Orru, *Angew. Chem., Int. Ed.*, 2013, **52**, 7084–7097 and references cited therein.

5 Y. Wang, H. Wang, J. L. Peng and Q. Zhu, *Org. Lett.*, 2011, **13**, 4604–4607.

6 B. Ma, Y. Wang, J. L. Peng and Q. Zhu, *J. Org. Chem.*, 2011, **76**, 6362–6366.

7 (*a*) M. Catellani and G. P. Chiusoli, *J. Organomet. Chem.*, 1992, **437**, 369–373; (*b*) C. C. Hughes and D. Trauner, *Angew. Chem., Int. Ed.*, 2002, **41**, 1569–1572; (*c*) B. S. Lane, M. A. Brown and D. Sames, *J. Am. Chem. Soc.*, 2005, **127**, 8050–8057; (*d*) E. J. Hennessy and S. L. Buchwald, *J. Am. Chem. Soc.*, 2003, **125**, 12084–12085.

8 Our recent theoretical study for the Cu- and Pd-catalyzed intramolecular C–H activation of *N*-arylamidines: J. Li, H. H. Gu, C. H. Wu and L. J. Du, *Dalton Trans.*, 2014, **43**, 16769–16779.

9 (*a*) S. L. Zhang, L. Shi and Y. Q. Ding, *J. Am. Chem. Soc.*, 2011, **133**, 20218–20229; (*b*) M. Gómez, J. Granell and M. Martinez, *Organometallics*, 1997, **16**, 2539–2546; (*c*) M. Gómez, J. Granell and M. Martinez, *J. Chem. Soc., Dalton Trans.*, 1998, 37–43.

10 (*a*) D. Babić, M. Ćurić and D. M. Smith, *J. Organomet. Chem.*, 2011, **696**, 661–669; (*b*) S. Rousseaux, M. Davi, J. Sofack-Kreutzer, C. Pierre, C. E. Kefalidis, E. Clot, K. Fagnou and O. Baudoin, *J. Am. Chem. Soc.*, 2010, **132**, 10706–10716; (*c*) M. Chaumontet, R. Piccardi, N. Audic, J. Hitce, J. L. Peglion, E. Clot and O. Baudoin, *J. Am. Chem. Soc.*, 2008, **130**, 15157–15166; (*d*) D. L. Davies, S. M. A. Donald and S. A. Macgregor, *J. Am. Chem. Soc.*, 2005, **127**, 13754–13755.

11 (*a*) A. J. Mota, A. Dedieu, C. Bour and J. Suffert, *J. Am. Chem. Soc.*, 2005, **127**, 7171–7182; (*b*) M. A. Campo, Q. H. Huang, T. L. Yao, Q. P. Tian and R. C. Larock, *J. Am. Chem. Soc.*, 2003, **125**, 11506–11507; (*c*) E. Capito, J. M. Brown and A. Ricci, *Chem. Commun.*, 2005, 1854–1856; (*d*) A. J. Canty and G. van Koten, *Acc. Chem. Res.*, 1995, **28**, 406–413.

12 (*a*) A. D. Becke, *J. Chem. Phys.*, 1993, **98**, 5648–5652; (*b*) C. Lee, W. Yang and R. G. Parr, *Phys. Rev. B: Condens. Matter*, 1988, **37**, 785–789; (*c*) P. J. Stephens, F. J. Devlin, C. F. Chabalowski and M. J. Frisch, *J. Phys. Chem.*, 1994, **98**, 11623–11627.

13 (*a*) K. Fukui, *J. Phys. Chem.*, 1970, **74**, 4161–4163; (*b*) K. Fukui, *Acc. Chem. Res.*, 1981, **14**, 363–368.

14 (*a*) P. J. Hay and W. R. Wadt, *J. Chem. Phys.*, 1985, **82**, 299–310; (*b*) W. R. Wadt and P. J. Hay, *J. Chem. Phys.*, 1985, **82**, 284–298.

15 A. W. Ehlers, M. Böhme, S. Dapprich, A. Gobbi, A. Höllwarth, V. Jonas, K. F. Köhler, R. Stegmann, A. Veldkamp and G. Frenking, *Chem. Phys. Lett.*, 1993, **208**, 111–114.

16 P. C. Hariharan and J. A. Pople, *Theor. Chim. Acta*, 1973, **28**, 213–222.

17 (*a*) V. Barone and M. Cossi, *J. Phys. Chem. A*, 1998, **102**, 1995–2001; (*b*) M. Cossi, N. Rega, G. Scalmani and V. Barone, *J. Comput. Chem.*, 2003, **24**, 669–681; (*c*) J. Tomasi, B. Mennucci and R. Cammi, *Chem. Rev.*, 2005, **105**, 2999–3093.

18 L. E. Roy, P. J. Hay and R. L. Martin, *J. Chem. Theory Comput.*, 2008, **4**, 1029–1031.

19 A. V. Marenich, C. J. Cramer and D. G. Truhlar, *J. Phys. Chem. B*, 2009, **113**, 6378–6396.

20 M. J. Frisch, *GAUSSIAN 09 (Revision C.01)*, Gaussian, Inc., Wallingford, CT, 2010, [Full reference given in the ESI†].

21 (*a*) S. Kozuch and S. Shaik, *Acc. Chem. Res.*, 2011, **44**, 101–110; (*b*) A. Uhe, S. Kozuch and S. Shaik, *J. Comput. Chem.*, 2011, **32**, 978–985.

22 D. Braga, F. Grepioni, E. Tedesco, K. Biradha and G. R. Desiraju, *Organometallics*, 1997, **16**, 1846–1856.